Von Willlebrand Adhesion to Surfaces at High Shear Rates Is Controlled by Long-Lived Bonds

Charles E. Sing,[†][*] Jennifer G. Selvidge,[‡] and Alfredo Alexander-Katz[‡]
[†]Department of Materials Science and Engineering, Northwestern University, Evanston, Illinois; and [‡]Department of Materials Science and Engineering, Massachusetts Institute of Technology, Cambridge, Massachusetts

ABSTRACT   Von Willebrand factor (vWF) adsorbs and immobilizes platelets at sites of injury under high-shear-rate conditions. It has been recently demonstrated that single vWF molecules only adsorb significantly to collagen above a threshold shear, and here we explain such counterintuitive behavior using a coarse-grained simulation and a phenomenological theory. We find that shear-induced adsorption only occurs if the vWF-surface bonds are slip-resistant such that force-induced unbinding is suppressed, which occurs in many biological bonds (i.e., catch bonds). Our results quantitatively match experimental observations and may be important to understand the activation and mechanical regulation of vWF activity during blood clotting.

INTRODUCTION

The large, multimeric protein von Willebrand factor (vWF) is known as one of the initial responders in the blood-clotting cascade (1–3). In particular, vWF provides the initial substrate upon which platelets accumulate at the site of a wounded blood vessel when there are large flow fields that prohibit the platelet-collagen interactions that initiate the clotting cascade in vessels with slower flow rates (1–4). This is known to occur through the glycoprotein-IIb-vWF-A1-domain interaction, which possesses a novel force response such that the ligand-receptor pair remains stable even under large forces (1–3,5–7). The subsequent integrin-RGD interactions between vWF and platelets completely arrest their motion at the surface (1,2). Although this process and the resulting clotting cascade are well studied in the literature (1,2), recent attention has focused on the initial vWF deposition (1–4,8,9).

vWF deposition is known to occur only at large shear rates, primarily due to the transition of vWF from a collapsed, globular conformation to an elongated network (1–4,8–10). In a pioneering work, Siedlicki et al. used atomic force microscopy to demonstrate that shear induces these conformational changes (8), and subsequent research has elaborated on this by considering in vitro systems (9,11). Cooperative effects can be seen in the multicomponent and concentrated biological systems, however these shear-responsive effects are seen even at the single-molecule level (9,12). Crucially, it is shown that there is a threshold shear rate above which drastic stretching and adsorption occur simultaneously in collagen-coated microfluidics channels (9). The prevailing conceptual picture, determined both from simulation and experiment, is that the elongational component of the flow initiates the conformational change of vWF through a nucleation-protru-sion mechanism that drives the initial stretching from a polymer in a globular geometry (9,13–15). At most, surface-induced effects such as enhanced unfolding can increase unfolding by a factor of 2 (16), but these effects fail to explain the sudden and rapid adsorption observed in experiments.

Simultaneous research into fluorescently labeled DNA molecules has elucidated the driving forces governing the adsorption and desorption of molecules in shear flows near surfaces; specifically, a powerful lift force drives the desorption and subsequent depletion of molecules that are stretched by shear flow (17–21). This lift force is a hydrodynamic effect seen in flow-stretched polymers that produces a force perpendicular to the applied shear flow, and it is due to local induced flows interacting with the no-slip boundary condition at the surface (17–21). Our recent research, informed by the same simulation model that successfully describes vWF stretching in earlier work, has mapped out the shear-induced desorption of a polymer globule, with Lennard-Jones type interactions between the surface and the polymer (22). The accompanying theory is based on the current understanding of the hydrodynamic lift force, and the results clearly indicate that shear-induced adsorption will never occur with this type of model (21,22). Although stretching the molecule induces a drastic increase in the number of binders (so the binding force, f, scales as the length, L, of the molecule, $f \sim L$), this is dwarfed by the opposing hydrodynamic lift force, f_L, which scales as $f_L \sim L^4$ (21,22).

The currently available models are thus not sufficient to explain the observed vWF adsorption process, even in straightforward in vitro situations. Here we demonstrate that introducing Bell-model-type interactions to these existing models allows the specification of the criterion for a shear-induced adsorption of a molecule such as vWF.

SIMULATION RESULTS

Bell model interactions incorporated Into Brownian dynamics

In biological systems where binding occurs through reversible ligand-receptor-type bonds, the Bell model is ubiquitous as a way to parameterize a more complicated energy landscape in a facile manner by defining interacting entities as either bound or unbound. (23) The rate of transition between the two states is governed by the height of an intermediate energy barrier between them, with a large barrier impeding both the forward and backward transitions and a small barrier allowing rapid binding and unbinding. This results in a bond that has a characteristic binding/unbinding time that is dependent on the energy barrier between the two states. We incorporate this Bell model into traditional Brownian dynamics simulations in a fashion reminiscent of similar models used in previous work by the authors and by others in the literature (24–27). Our methods are described in detail in the Appendix.

In Fig. 1, *a* and *b*, we conceptually demonstrate how we implement a general Bell model into our simulations (22,24). The simplified energy landscape assumed in the Bell model is parameterized by a bound state with energy E_B and position r_B, an unbound state with energy E_{UB} and position r_{UB}, and the energy difference between the bound state and the transition state, $\Delta E_{UB,0}$. The transition state, in principle, has a position r^* as well; we examine two situations in this article, $r^* = r_{UB}$ (Fig. 1 *a*) and $r^* = r_B$ (Fig. 1 *b*). In equilibrium, this location is arbitrary, but under an applied force, the tilting of the energy landscape (Fig. 1, *a* and *b*, *blue lines*) can alter the height of the energy barrier, $\Delta E_{UB,f}$, relative to the zero-force unbinding energy, $\Delta E_{UB,0}$. In the $r^* = r_{UB}$ case, $\Delta E_{UB,f}$ is decreased upon application of force, resulting in well-known slip-bond behavior (6,23). Alternatively, if $r^* = r_B$, the zero-force unbinding energy is unaffected by force, $\Delta E_{UB,f} = \Delta E_{UB,0}$, resulting in what we call suppressed slip-bond behavior. In principle,

$r^* < r_B$ would yield catch-bond behavior, where the bond lifetime increases upon application of force; this would be a continuation of proceeding from the slip bond to the suppressed-slip-bond situation. We note that the position r^* is a phenomenological parameter that is a minimal way to account for the complicated atomic-level processes that lead to a given force response. Other, more complex scenarios may occur, yet here we want to make a plausibility statement rather than include multiple variables that are experimentally unknown for this system. For our model, we consider $\Delta \tilde{E}_B$ to be force-independent, since characteristics affecting binding rate, such as lift-force-induced depletion, are included explicitly in the simulation and should not be reconsidered at the local interaction level. It is in principle possible that force could alter the conformational aspects of the associating units in the unbound state, but we do not include such modifications, since they are as yet unknown for this particular system. We expect that the qualitative behavior would be the same.

Since Lennard-Jones models seem sufficient to describe single-chain behavior away from an attractive surface (9), we only incorporate Bell model associations into polymer-surface interactions. For vWF, these represent collagen-A3 interactions, whose nature has still not been completely elucidated (28,29). Therefore, although we have no direct experimental values to direct the parameterization of our Bell model energy landscape, we explore the effect of its parameters on the adsorption behavior of our model to provide predictions for what behaviors to expect. To carry this out, we characterize a number of equilibrium binding energies of association of vWF to the surface, $\Delta E_0 = E_B - E_{UB}$ (where a decrease in ΔE_0 indicates an increased preference for the bound state) (22–24), and investigate the remaining Bell model parameters. We choose the equilibrium unbinding time $\tau_{UB} = \nu_0 e^{\Delta E_{UB,0}/(k_B T)}$ and the barrier location with respect to the bound state, $r^* - r_B$ (from now on we use the convention $r_B = 0$). The former is chosen due to its invariance to the particular choice of ν_0 (which in the
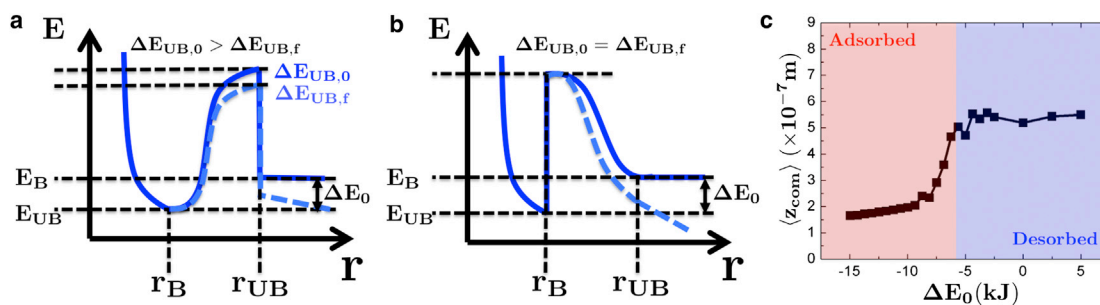

FIGURE 1   (*a* and *b*) Schematics of the Bell model reaction landscape for extreme slip-bond behavior (*a*) and suppressed slip-bond behavior (*b*). There is a bound state with energy E_B at position r_B and an unbound state with energy E_{UB} at position r_{UB}. The barrier between these states can be characterized with the energy difference ΔE_{UB} measured with respect to E_B. In *a*, this barrier is positioned at $r^* = r_{UB}$ for extreme slip-bond behavior, such that application of force (*blue line*) decreases the barrier from $\Delta E_{UB,0}$ to $\Delta E_{UB,f}$. In *b*, the energy barrier is positioned at $r^* = r_B$, such that $\Delta E_{UB,0} = \Delta E_{UB,f}$. (*c*) Equilibrium behavior of a polymer ($N = 50$, $\tilde{u} = 2.08$) near a surface. The center of mass of the polymer ($\langle z_{com} \rangle$) is measured versus the binding energy, $\Delta E_0 = E_B - E_{UB}$, with the surface (values demonstrated are negative in sign). Large values of $\langle z_{com} \rangle$ indicate desorbed states that are of interest in this article.

simulation is chosen out of convenience) (30) and allows the probing of long-lived binding states; the latter determines the force response of the energy barrier, allowing us to investigate the ramifications of slip versus non-slip bonds. For a given unbinding time, the choice of barrier energy, $\Delta E_{UB,0}$, and $n\nu_0$ are arbitrary, since replacement of $\Delta E_{UB,0} = \Delta E_{UB,0,new} + \delta E_{UB}$ yields $\tau_{UB} = \nu_0 e^{-E_{UB,0}/(k_BT)} = \nu_0 e^{-\delta E_{UB}/(k_BT)} e^{-E_{UB,0,new}/(k_BT)} = \nu_{0,new} e^{-E_{UB,0,new}/(k_BT)}$, where $\nu_{0,new} = \nu_0 e^{-\delta E_{UB}/(k_BT)}$. For our simulations, $n\nu_0$ is chosen for convenience such that it is quick relative to the timescale of the induced flow but slow enough to allow good time averages of values used to calculate force corrections to $\Delta E_{UB,0}$. Due to the arbitrary nature of these choices, we represent the comparisons between different binding barriers as comparisons between different binding timescales, as this is a nonambiguous value.)

Results

In Figs. 1 c and 2, we demonstrate the effect of changing these parameters on the behavior of a single polymer chain near a surface. Fig. 1 c provides the equilibrium context; the height of the polymer at the surface $\langle z_{com} \rangle$ is plotted as a function of the energy difference between the bound and unbound states, ΔE_0. For sampling purposes, the polymer is restricted to heights $< 9.5 \times 10^{-7}$ m away from the surface by an applied potential, and the system is run for ≈ 100 times the total relaxation time of the chain z-position. At $\Delta E_0 > -5$ kJ/mol, the vWF in equilibrium no longer associates permanently with the surface and is thus in the desorbed state. This is the state in which vWF is observed in experiment, so we focus our efforts on this regime.

Upon establishing the equilibrium behavior of the polymer as being in the experimentally relevant desorbed regime, we investigate the dynamics of the system upon applying a simple shear flow and examining the influence of binding lifetimes. In Fig. 2, simulation results demonstrate this influence by altering the lifetime of the bond for the case $r^* = 0$ nm by plotting vWF height

$\langle z_{com} \rangle$ as a function of shear rate $\dot\gamma$ for a number of binding energies, ΔE_0. Fig. 2 a demonstrates the shortest binding timescale, $\tau_{UB} = 0.42$ ms. At no shear rate $\dot\gamma$ or binding energy ΔE_0 tested does the vWF model increasingly localize at the surface, but the bound states of $\Delta E_0 = -5$ kJ/mol and $\Delta E_0 = -3.75$ kJ/mol suggest that there may be a low (but finite) $\dot\gamma$ adsorption that we revisit in our theoretical discussion. It is important to note that vWF indeed gets pushed farther away as the shear rate is increased due to an increase in the hydrodynamic lift force. The limiting case for this behavior is essentially identical to that for a Lennard-Jones model of vWF (22,24), and it demonstrates the lack of a shear-induced adsorption for situations where the polymer-surface binding lifetimes are small. In Fig. 2, b and c, the lifetime of the bond increases by a factor of $e^2 = 7.4$, corresponding to a barrier height increase of $2k_BT \approx 5$ kJ/mol. For Fig. 2 b, the increase in binding time results in an intermediate shear rate regime where vWF becomes bound to the surface, but at large values of shear rate or large values of ΔE_0, the polymer remains unbound. This window occurs in $\dot\gamma \approx 10^3 - 10^4 s^{-1}$, and is modest for both $\Delta E_0 = -2.5$ kJ/mol and $\Delta E_0 = -3.75$ kJ/mol. Such behavior is more pronounced in Fig. 2 c, which has both long binding behavior and suppressed slip-bond behavior ($r^* = 0$); this demonstrates the shear-induced adsorption behavior experimentally observed to occur in vWF. For contrast, vWF that binds to the surface with slip bonds ($r^* = 10$ nm) is also shown for the same binding energies and unbinding timescales as in Fig. 2 c. No shear-induced adsorption is observed, illustrating the requirement that slip-bond behavior be strongly suppressed to reproduce vWF behavior. This amounts to what is essentially a prediction for the limiting behavior of expected behavior of the A3-collagen interaction, which is that the bond must be either a no-slip bond or even a catch bond to counteract the lift-force-induced desorption. This will be articulated further in our theoretical arguments.

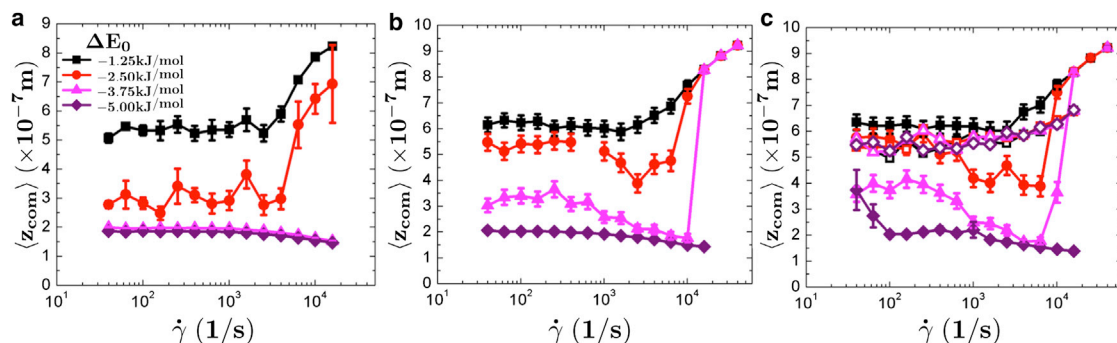We demonstrate that this model indeed reproduces the experimental observation that vWF stretching and

FIGURE 2 Plots of the average z center of mass of our vWF model ($\langle z_{com} \rangle$) as a function of shear rate, $\dot\gamma$. Each graph corresponds to a different unbinding time: $\tau = 0.416$ ms (a), 3.07 ms (b), and 22.7 ms (c). Curves with solid symbols correspond to the legend and indicate the condition $r^* = 0$ nm. Curves with open symbols in c correspond to $r^* = 4$ nm for the same conditions, to contrast the profound effect of r^* on adsorption ability. Shear-induced adsorption (desorbed → adsorbed) is seen only at large τ_{UB} and low r^* (b and c).

adsorption occur concurrently, as shown in Fig. 3, which plots both the fraction of time that at least 10 binders are bound (f_{B10}) and the normalized extension length of the molecule $\langle L_x \rangle / L$ as a function of shear rate $\dot{\gamma}$. These responses are representative of the experimental data shown in Schneider et al., with both qualitative and quantitative matching for both curves (9). Although previous explanations relied primarily on the extension data, which indeed match for certain simple simulation and theoretical models based on globule-stretch transitions (9,14,15), the additional matching to adsorption data is significant, as these models do not address the powerful hydrodynamic lift force apparent in Fig. 2. Furthermore, simulation realization of the curves in Schneider et al. produces predictions about the nature of the vWF-surface interactions, namely, that they should be long-lived and non-slip bonds if this model is indeed valid. To further articulate these points, we consider a straightforward quantitative argument that clarifies the role of these aspects of the interaction.

Alternative explanations for the observed phenomena are possible, but most fall short in one aspect of the experimental observations. Extremely long-lived slip bonds, such that the lift-force-driven unbinding is insufficient to remove the bond, are typically also strong bonds that would cause even a collapsed vWF molecule to bind almost irreversibly to the surface. This is not observed in experiment, since vWF molecules are not bound unless they are sheared (9). A series of bonds with different chemical functionality, i.e., a quick, strong, but short-lived bond leading to a strong, more long-lived bond that stabilizes vWF-surface interactions is unsupported by the literature, since the A3-collagen association is the sole interaction in the initial adsorption process (28,29). Although more complicated surface interactions may be possible, this minimalist model indeed
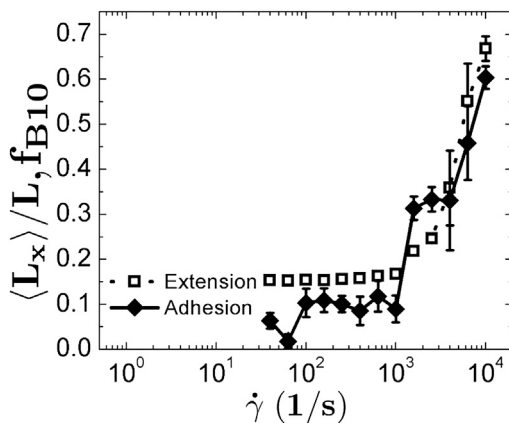
captures the salient features observed in vWF adsorption experiments (9).

THEORY FOR SHEAR-INDUCED ADSORPTION

Fig. 4 demonstrates a simplified three-state model of collapsed polymers that can adsorb with an attractive surface, with the states corresponding to the desorbed globule state (d), the adsorbed globule state (g), and the adsorbed stretched state (s). Transitions between two states, i and j, can be represented by a jump frequency, ν_{ij}, which describes the evolution of the system through states with populations n_i and n_j using the well-known master equation

$$\frac{\partial n_i}{\partial t} = \sum_j \nu_{ij} n_j. \tag{1}$$

We consider only three states and focus in particular on the frequency of entrance and departure from the adsorbed stretched state (s) under a steady-state assumption (drawn schematically in Fig. 4),

$$n_s \left[\nu_{sd} + \nu_{sg} \right] = (1 - n_s) \nu_{gs}, \tag{2}$$

where n_s is the fraction of the molecule in the adsorbed stretched state. The various transition frequencies are given by the relaxation times for each of the processes. The characteristic time of globule stretching and binding ($1/\nu_{gs} \sim 1/C[1/\dot{\gamma} + \tau_{UB} e^{\Delta E_0 / k_B T}]$) is given by the inverse of the shear rate (unfolding driven by the fluid flow) and subsequently the characteristic binding time, $\tau_{UB} e^{\Delta E_0 / k_B T}$. The constant $C \ll 1$ is important to include, since it represents the fraction of molecules in the adsorbed globule state as opposed to the desorbed state and should be extremely small in a system that is not strongly adsorbed at the surface in equilibrium, such as the situations where

FIGURE 3 Fractional extension, $\langle L_x \rangle / L$, and normalized adsorption, f_{B10} (described in Simulation Results), as a function of shear rate $\dot{\gamma}$. At a critical shear rate between 10^3 s^{-1} and 10^4 s^{-1}, both extension and adsorption drastically increase. This corresponds directly with experimental data given in Schneider et al., which are not plotted here but can be found in the original article (9).
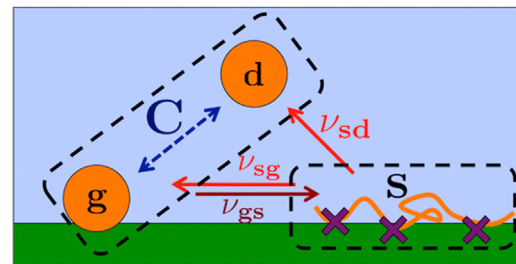

FIGURE 4 Schematic of the three-state model used to conceptually illustrate the shear-induced adsorption behavior of vWF. vWF can be in either a desorbed state (d), an adsorbed globule state (g), or a stretched and adsorbed state (s). We focus on the transitions between the s state and the combined d and g states. Small values of r^* and τ_{UB} suppress the transitions leaving the s state (ν_{sd} and $\nu_{gs} \rightarrow 0$) but do not adversely affect the ν_{sg} transition, so there is then a net accumulation in the s state. The coefficient C describes the fraction of bound states within the combined g-d space, which may change with shear rate and equilibrium binding energies.

$\Delta E_0 > -5.0$ kJ/mol in Fig. 2, *a–c*. In reality, this value will shrink with larger values of $\dot{\gamma}$ due to the hydrodynamic lift force, though extension at the surface typically occurs well before this transition takes place in the bulk (22). The characteristic time of both the lift force and the recollapse transition are given by the unbinding time of *n* binding locations plus the movement driven by the shear rate ($1/\nu_{sd} \sim 1/\nu_{sg} \sim \tau_{UB}^n e^{-f(\dot{\gamma},n^4)r^*/k_BT} + 1/\dot{\gamma}$). We emphasize the large value of the force in this expression, which we have written as a function of n^4 due to the assumption that $L \sim n$. This is where the detachment due to the lift force plays a major role, as the elongated nature of the molecule results in the strong upward force that applies a large force to the vWF-surface binding. Only upon unbinding of all the associations can the vWF proceed to either roll back into a collapsed state or lift away from the surface. This large increase with the number of binders quickly drives the timescale of the unbinding transitions, $1/\nu_{sd} \sim 1/\nu_{sg} \to 0$. The expressions for ν_{ij} can be incorporated into Eq. 2 to yield the overall fraction of adsorbed material:

$$n_s \sim \cfrac{1}{\cfrac{2}{C}\left[\cfrac{\frac{1}{\dot{\gamma}} + \tau_{UB}e^{\Delta E_0/k_BT}}{\frac{1}{\dot{\gamma}} + \tau_{UB}^n \nu_0^{n-1} e^{-f(\dot{\gamma},n^4)r^*/k_BT}}\right] + 1}. \qquad (3)$$

We have ignored many of the coefficients, and we consider these to be of order unity, as this work is intended to present a conceptual rather than a quantitative argument.

Assumed in this manifestation of ν_{gs} is the discretization into a singly binding globule versus a highly bound stretched chain. As $\tau_{UB}e^{\Delta E_0}$ is decreased, this discretization becomes less pronounced due to a nonnegligible fraction of times that the globule would be driven in a doubly or triply bound state due to small amounts of shear. This would increase the phase space open to the globule state and increase the bound fraction (especially in the vicinity of the adsorption transition). This is observed in the low-$\tilde{\dot{\gamma}}$ regime in Fig. 2, *a* and *b*, and in the $\Delta E_0 = -5.0$ kJ/mol traces for all plots, but it is not a pronounced effect at longer unbinding times τ_{UB}, such as in Fig. 2 *c*, which we postulate is closer to physical reality.

The limits of Eq. 3 are instructive for the relevant situation of $C \ll 1$. The largest effect is due to the interplay between the lifetime of binding, τ_{UB}, and the barrier location, r^*. To do this, we focus on the high $\dot{\gamma}$ situation (at small $\dot{\gamma}$, the bracketed term is ≈ 1 and $n_s \approx 0$). For the case where r^* is large, the bracketed term is dominated by the lift force, f_L (which grows quickly with n^4, since $n \sim L$), which is large, such that $n_s \to 0$. Likewise, even if $r^* = 0$, a small τ_{UB} will render the bracketed value of order 1. Since C is small, $n_s \approx 0$. Only through the combined influence of $r^* \to 0$ and a large τ_{UB} will $n_s \to 1$ (a shear-induced adsorption).

These limiting statements qualitatively reinforce the observations in simulation data. The shear-induced adsorption only occurs at large values of τ_{UB}, which drive $n_s \to 1$ due to its suppression of the transitions away from the stretched, adsorbed state without affecting the transitions into the same state. This suppression can be counteracted if there is a large lift force pulling the polymer away from the surface, $f \to \infty$, which occurs upon extension. This force can act strongly upon the binding interactions, but if $r^* \le 0$ (i.e., in the case of a catch or no-slip bond), this effect can be rendered negligible. We emphasize that this represents a theoretical argument that is not intended for quantitative matching; coefficients are left out or represented very generally, and phase space is discretized in an imprecise way. Nonetheless, the competition between shear timescales ($1/\dot{\gamma}$) and unbinding timescales ($\tau_{UB}^n \nu_0^{n-1} \exp(-fr^*/k_BT)$) captures the essence of the simulation observations, as does the competition between the unbinding timescales and lift forces ($\tau_{UB}^n \nu_0^{n-1} \exp(-fr^*/k_BT)$).

CONCLUSION

Simulation data, combined with straightforward theoretical arguments, clarify the essential physics that must be involved with vWF function; specifically, the slip-bond behavior must be suppressed ($r^* \to 0$) and the unbinding time must be large ($\tau_{UB}^n \gg 1/\dot{\gamma}$). This ensures that upon the occasion that a vWF molecule interacts with the surface, there is a suppression of the pathways for unbinding from the surface due to the lift force and/or rolling pathways. This general assertion is backed up by experiment upon comparison of the data in Fig. 3 with labeled vWF in Schneider et al. (9), as well as the observation in the same article that adsorbed vWF is translationally static, which can be shown to require long-lived binding kinetics (22). We have therefore proposed a straightforward set of criteria for a simple vWF model to show the expected shear-induced adsorption behavior, and to our knowledge, we have the only model currently that indeed shows the presence of such a transition.

APPENDIX A: SIMULATION METHODS

Brownian dynamics with Bell model interactions

In modeling the vWF chain as a homopolymer near an attractive surface, we use a Brownian dynamics simulation that involves numerically integrating the movement of a bead *i* at location r_i through a discretized Langevin equation:

$$\Delta \tilde{r}_i = \Delta \tilde{t} \left(\tilde{v}_\infty - \sum_j^N \tilde{\mu}_{i,j} \cdot \nabla \tilde{U}_j \right) + \zeta_j, \qquad (4)$$

where $\tilde{\mu}_{ij}$ is the hydrodynamic mobility tensor, which has either the form $\tilde{\mu}_{i,j} = \delta_{i,j}\,\mathbf{I}6\pi\eta a$ (the freely draining approximation) for measurement of equilibrium values or the Rotne-Prager-Yamakawa-Blake tensor (31–33)

for assessment of dynamic situations (e.g., including shear flows). The Rotne-Prager-Yamakawa-Blake tensor is used in all dynamic situations, because it accurately describes the hydrodynamic interactions and no-slip boundary conditions that are necessary to reproduce the correct flow environment (in particular, the hydrodynamic lift force). $\delta_{i,j}$ represents the Kronecker delta, $\mathbf{I}$ is the identity tensor, and a represents the bead radius. ζ_j is a randomly generated noise velocity that satisfies the fluctuation-dissipation theorem, $\langle \zeta_i(t)\zeta_j(t')\rangle = 2k_BT\delta_{ij}\delta(t-t')\tilde{\mu}_{ij}$, and $\tilde{v}_\infty$ is the applied fluid flow (in this article, $\tilde{v}_\infty = \tilde{\tilde{\gamma}}(r_{i,z}-3.0)\Theta(r_{i,z}-3.0)\widehat{\mathbf{e}}_{\mathbf{x}}$, which is a shear flow in the direction of the unit vector $\widehat{\mathbf{e}}_{\mathbf{x}}$). Tildes signify that a quantity has been rendered dimensionless through comparisons to the thermal energy k_BT, the bead radius a, and the diffusion time of a single bead $\tau = 6\,\pi\eta\,a^3/(k_BT)$.

The potential term $\tilde{U}$ is composed of several distinct components—the intrapolymeric Lennard-Jones interactions, $\tilde{U}_{LJ}$; interactions between connected beads along the chain, $\tilde{U}_C$; surface interactions, $\tilde{U}_S$; and a wall potential, $\tilde{U}_W$ —introduced to keep the polymer within the relevant volume:

$$\tilde{U} = \tilde{U}_{LJ} + \tilde{U}_C + \tilde{U}_S + \tilde{U}_W$$

$$= \tilde{u}\sum_{ij}\left(\left(\frac{2}{\tilde{r}_{ij}}\right)^{12} - 2\left(\frac{2}{\tilde{r}_{ij}}\right)^6\right) + \frac{\tilde{\kappa}}{2}\sum_{i}^{N-1}(\tilde{r}_{i+1,i}-2)^2$$

$$+\frac{\tilde{\kappa}}{2}\sum_{i,j}^{N,N_B}\omega_{i,j,t}\tilde{r}_{i,j}^2 + \sum_{i}(3\ln(\tilde{r}_{i,z}-1)-1.5\tilde{r}_{i,z}$$

$$-3(\ln 2-1))\Theta(3-\tilde{r}_{i,z}),$$

where each contribution is listed in the order denoted immediately after the first equal sign. In this equation, $\tilde{u}$ dictates the relative strength of the Lennard-Jones interactions, with larger values of $\tilde{u}$ indicating larger attraction between adjacent beads i and j. $\tilde{u} = 0.41$ is known to be a theta polymer at all values, N, and values of $\tilde{u}>0.66$ drive an $N = 50$ polymer into a globular conformation (34). In line with previous literature, we choose $\tilde{u} = 2.08$, since it has been demonstrated to represent well the shear response of vWF in in vitro experiments (9). $r_{ij} = |\mathbf{r}_i - \mathbf{r}_j|$ represents the distance between two beads, i and j. Chain and surface-association connectivity are enforced by a harmonic spring potential, with a spring constant of $\tilde{\kappa} = 200.0$ that is chosen to render bond stretching negligible. We note that this represents a constraint on the system and not the binding energy at the surface, which is incorporated into the simulation through the Bell model statistics. The final component of the potential, $\tilde{U}_W$, is the wall force, in which $r_{i,z}$ represents the z height from the surface at $z = 0$ and the binders are at $z = 3$. This term is chosen so that it is a $1/(\tilde{r}_{i,z}-1)$ scaling for the force ($-\partial\tilde{U}/\partial\tilde{r}_{i,z}$), such that $\tilde{U}_W = 0$ and $-\partial\tilde{U}/\partial\tilde{r}_{i,z} = 0$ for $\tilde{r}_{i,z} = 3.0$. The wall force constrains the polymer to the area above $z>0$, and the exact form of this potential has negligible impact on the simulation results.

The surface contribution, $\tilde{U}_S = \tilde{\kappa}\sum_{ij}^{N,N_B}\omega_{i,j,t}\tilde{r}_{i,j}^2/2$, considers the binding interaction between each bead and each binder. Four hundred binders are randomly placed on a $100a \times 40a$ area, where binders can be no closer together than two bead radii. This density is arbitrarily chosen, but is large enough that at full extension, a single vWF molecule can associate with a large number of binders simultaneously. This is meant to reproduce the A3-collagen interaction, which is still poorly defined (28,29), so it is unclear how appropriate this value is. Unpublished results suggest that the response to changes in density and distribution of surface binders is not extremely sensitive in this dense-binder regime, but more elaborate models that allow for binder-binder cooperativity and large-scale inhomogeneity could in principle be incorporated (22). This surface is rendered infinite through the imposition of periodic boundary conditions.

Bead-surface interactions occur through the well-known Bell model, which involves the inclusion of the time-varying $\omega_{i,j,t}$ matrix (24). The matrix $\omega_{i,j,t}$ is an accounting of the status of binding between a polymer bead i and a surface binder j at time t, with a 1 indicating that there is

binding and a 0 indicating the absence of a binding interaction. These are probabilistically turned on and off for when a bead is in close proximity to a binder, indicating binding or unbinding reactions, with reaction updates occurring every time interval $\tau_0 = 1/\nu_0$. The Monte Carlo type update step is governed by

$$\omega_{i,j,t} = \begin{cases} \begin{cases} 1\ if\ \Xi < e^{-\Delta\tilde{E}_{UB,0}-\Delta\tilde{E}_0} \\ 0\ if\ \Xi > e^{-\Delta\tilde{E}_{UB,0}-\Delta\tilde{E}_0} \end{cases} & if\ \omega_{i,j,t-\tau_0} = 0\cap\tilde{r}_{i,j}\leq\tilde{r}_{rxn} \\ \begin{cases} 0\ if\ \Xi < e^{-\Delta\tilde{E}_{UB,0}+\langle\tilde{f}\rangle\tilde{r}^*} \\ 1\ if\ \Xi > e^{-\Delta\tilde{E}_{UB,0}+\langle\tilde{f}\rangle\tilde{r}^*} \end{cases} & if\ \omega_{i,j,t-\tau_0} = 1 \end{cases},$$

where the values $\Delta\tilde{E}_{UB,0}$ and $\Delta\tilde{E}_0$ were defined earlier, in Fig. 1. Here, $\tilde{r}_{rxn} = 1.0$ is the radius within which a reaction may occur between the monomer and the surface binder. This value is chosen to represent a binding volume similar to that found in similar models (24). Ξ is a randomly generated number between 0 and 1 that is compared to the probability of binding and unbinding ($e^{-\Delta\tilde{E}_B}$ and $e^{-\Delta\tilde{E}_{UB}+\langle\tilde{f}\rangle\tilde{r}^*}$, respectively), which are functions of the energy of binding, $\Delta\tilde{E}_B$, and unbinding, $\Delta\tilde{E}_{UB}$. The applied force $\langle\tilde{f}\rangle$ along a polymer-binder interaction may also affect the unbinding behavior of that association through the force-distance contribution, $\langle\tilde{f}\rangle\tilde{r}^*$, in the aforementioned unbinding probability, where $\tilde{r}^*$ is either $\tilde{r}^* = 0.1$ (slip bond) or $\tilde{r}^* = 0.0$ (non-slip bond). The overall binding energy of the system, $\Delta\tilde{E}_B - \Delta\tilde{E}_{UB}$, governs the equilibrium behavior of the system.

For our simulations, $\tau_0 = 25\Delta\tilde{t}$, $\Delta\tilde{t} = 0.0001\tau$, $\tilde{u} = 0.41$, and $N = 50$, and each condition is run for at least 3×10^9 time steps (~100 times the relaxation time of the longest-relaxing system, measured by the time-time correlation function of $\tilde{r}_{com,z}$).

Correspondence of simulation values to real values

For simulation convenience, it is useful and conventional to describe the system in dimensionless variables. In our simulation, energies are rendered dimensionless using units of thermal energy, $\tilde{E}\to E/(k_BT)$, distances in units of dimer radius, $\tilde{r}\to r/a$, and times in units of the characteristic diffusion time, $\tilde{t}\to k_BTt/(6\pi\eta a^3)$ (where η is the solvent viscosity). To compare these dimensionless simulation results to vWF observations in experiment, we carry out the reverse transformations using relevant values of the various parameters. For the thermal energy, we represent energies in kJ/mol, using $RT = 8.31\ J/(K\times mol)\times 300\ K$. The dimer radius we use is 38 nm, which matches experimental observation (3). Finally, we use $\eta = 0.001\ Pa\cdot s$ as the viscosity of water. These are the only parameters that are needed to reinstate experimental dimensions to simulation results.

REFERENCES

1. Sadler, J. E. 1998. Biochemistry and genetics of von Willebrand factor. *Annu. Rev. Biochem.* 67:395–424.

2. Reininger, A. J. 2008. Function of von Willebrand factor in haemostasis and thrombosis. *Haemophilia.* 14 (*Suppl 5*):11–26.

3. Springer, T. A. 2011. Biology and physics of von Willebrand factor concatamers. *J. Thromb. Haemost.* 9 (*Suppl 1*):130–143.

4. Goerge, T., F. Kleinerüschkamp, …, S. W. Schneider. 2007. Microfluidic reveals generation of platelet-strings on tumor-activated endothelium. *Thromb. Haemost.* 98:283–286.

5. Kim, J., C. Z. Zhang, …, T. A. Springer. 2010. A mechanically stabilized receptor-ligand flex-bond important in the vasculature. *Nature.* 466:992–995.

6. Thomas, W. E. 2009. Mechanochemistry of receptor-ligand bonds. *Curr. Opin. Struct. Biol.* 19:50–55.

7. Huizinga, E. G., S. Tsuji, …, P. Gros. 2002. Structures of glycoprotein Ibα and its complex with von Willebrand factor A1 domain. *Science.* 297:1176–1179.

8. Siedlecki, C. A., B. J. Lestini, …, R. E. Marchant. 1996. Shear-dependent changes in the three-dimensional structure of human von Willebrand factor. *Blood.* 88:2939–2950.

9. Schneider, S. W., S. Nuschele, …, M. F. Schneider. 2007. Shear-induced unfolding triggers adhesion of von Willebrand factor fibers. *Proc. Natl. Acad. Sci. USA.* 104:7899–7903.

10. Zhang, X., K. Halvorsen, …, T. A. Springer. 2009. Mechanoenzymatic cleavage of the ultralarge vascular protein von Willebrand factor. *Science.* 324:1330–1334.

11. Nesbitt, W. S., E. Westein, …, S. P. Jackson. 2009. A shear gradient-dependent platelet aggregation mechanism drives thrombus formation. *Nat. Med.* 15:665–673.

12. Chen, H., M. A. Fallah, …, A. Alexander-Katz. 2013. Blood-clotting-inspired reversible polymer-colloid composite assembly in flow. *Nat. Commun.* 4:1333.

13. Alexander-Katz, A., M. F. Schneider, …, R. R. Netz. 2006. Shear-flow-induced unfolding of polymeric globules. *Phys. Rev. Lett.* 97:138101.

14. Sing, C. E., and A. Alexander-Katz. 2010. Elongational flow induces the unfolding of von Willebrand factor at physiological flow rates. *Biophys. J.* 98:L35–L37.

15. Sing, C. E., and A. Alexander-Katz. 2011. Dynamics of collapsed polymers under the simultaneous influence of elongational and shear flows. *J. Chem. Phys.* 135:014902.

16. Alexander-Katz, A., and R. R. Netz. 2007. Surface-enhanced unfolding of collapsed polymers in shear flow. *Europhys. Lett.* 80:18001.

17. Jendrejack, R. M., E. T. Dimalanta, …, J. J. de Pablo. 2003. DNA dynamics in a microchannel. *Phys. Rev. Lett.* 91:038102.

18. Ma, H. B., and M. D. Graham. 2005. Theory of shear-induced migration in dilute polymer solutions near solid boundaries. *Phys. Fluids.* 17:083103.

19. Serr, A., C. Sendner, …, R. R. Netz. 2010. Single-polymer adsorption in shear: flattening vs. hydrodynamic lift and surface potential corrugation effects. *Europhys. Lett.* 92:38002.

20. Sendner, C., and R. R. Netz. 2008. Shear-induced repulsion of a semi-flexible polymer from a wall. *Europhys. Lett.* 81:54006.

21. Sing, C. E., and A. Alexander-Katz. 2011. Non-monotonic hydrodynamic lift force on highly extended polymers near surfaces. *Europhys. Lett.* 95:48001.

22. Sing, C. E. 2012. Blood clotting inspired polymer physics. PhD thesis. Massachusetts Institute of Technology, Cambridge, MA.

23. Bell, G. I. 1978. Models for the specific adhesion of cells to cells. *Science.* 200:618–627.

24. Sing, C. E., and A. Alexander-Katz. 2011. Equilibrium structure and dynamics of self-associating single polymers. *Macromolecules.* 44:6962–6971.

25. Hoy, R. S., and G. H. Fredrickson. 2009. Thermoreversible associating polymer networks. I. Interplay of thermodynamics, chemical kinetics, and polymer physics. *J. Chem. Phys.* 131:224902.

26. Salib, I. G., G. V. Kolmakov, …, A. C. Balazs. 2011. Using mesoscopic models to design strong and tough biomimetic polymer networks. *Langmuir.* 27:13796–13805.

27. Korn, C., and U. S. Schwarz. 2006. Efficiency of initiating cell adhesion in hydrodynamic flow. *Phys. Rev. Lett.* 97:138103.

28. Farndale, R. W., J. J. Sixma, …, P. G. de Groot. 2004. The role of collagen in thrombosis and hemostasis. *J. Thromb. Haemost.* 2:561–573.

29. Romijn, R. A., E. Westein, …, E. G. Huizinga. 2003. Mapping the collagen-binding site in the von Willebrand factor-A3 domain. *J. Biol. Chem.* 278:15035–15039.

30. Reference deleted in proof.

31. Rotne, J., and S. Prager. 1969. Variational treatment of hydrodynamic interaction in polymers. *J. Chem. Phys.* 50:4831–4837.

32. Yamakawa, H. 1970. Transport properties of polymer chains in dilute solution: hydrodynamic interaction. *J. Chem. Phys.* 53:436–443.

33. Blake, J. R., and A. T. Chwang. 1974. Fundamental singularities of viscous flow. Part I: The image systems in the vicinity of a stationary no-slip boundary. *J. Eng. Math.* 8:23–29.

34. Alexander-Katz, A., and R. R. Netz. 2008. Dynamics and instabilities of collapsed polymers in shear flow. *Macromolecules.* 41:3363–3374.